Proceeding of the Korean Nuclear Society Autumn Meeting
Taejon, Korea, October 1996

Critical Heat Flux and Flow Pattern for Water Flow in Annular Geometry

Jae-Wook Park*, Won-Pil Baek and Soon Heung Chang
Korea Advanced Institute of Science and Technology

Abstract

An experimental study on critical heat flux (CHF) and two-phase flow visualization has been performed for water flow in internally-heated, vertical, concentric annuli under near atmospheric pressure. Tests have been done under stable forced-circulation, upward and downward flow conditions with three test sections of relatively large gap widths (heated length = 0.6 m, inner diameter = 19 mm, outer diameter = 29, 35 and 51 mm). The outer wall of the test section was made up of the transparent Pyrex tube to allow the observation of flow patterns near the CHF occurrence. The CHF mechanism was changed in the order of flooding, churn-to-annular flow transition, and local dryout under a large bubble in churn flow as the flow rate was increased from zero to higher values. Observed parametric trends are consistent with the previous understanding except that the CHF for downward flow is considerably lower than that for upward flow.

Introduction

The research on critical heat flux (CHF) has been extensively carried out during the last few decades for various geometries: round tubes, rod-bundles, annuli, rectangular channels, etc. A significant amount of work has been done for annular channels in the nuclear context, because they are, essentially, a "one-rod bundle" and may therefore be deemed to simulate more closely the rod bundle geometry than do round tubes (Hewitt, 1982). The investigation on the effect of the unheated outer wall in an internally heated annulus also provides insights into the cold wall effects in rod bundles. Some of the early CHF correlations for rod bundles were developed based on the annulus CHF data (Jannsen and Kervinen, 1963).

During the last 15 years, there have been significant work on the CHF in annuli at low pressure and low flow (LPLF) conditions which are relevant to some research reactors or heating reactors. Table 1 summarizes the experimental conditions of Mishima and Ishii (1982), Rogers et al. (1982), and El-Genk et al. (1988). Mishima and Ishii (1982) performed CHF tests for very low flow of water in an internally heated vertical annulus with a narrow gap (δ = 0.00275 m). The CHF was much lower than that predicted by conventional correlations but was well predicted by the churn-to-annular flow regime transition criterion. Rogers et al. (1982) performed tests with three vertical test sections (δ = 0.00445, 0.00595, 0.00855 m) to obtain the data for heating reactor design. Their data cover a somewhat large range of mass fluxes at subcooled and low quality conditions. In their tests, the dryout of the liquid film surrounding a slug flow bubble was the main CHF mechanisms, with the CHF values much lower than the predictions by conventional correlations. In addition, they suggested the boundary of the low flow region as G = 180 kg/m^{2}s, i.e., the condition that the inlet liquid velocity equals to the rise velocity of slug flow bubbles. El-Genk et al. (1988) performed the tests with three vertical annular channels (δ = 0.00365, 0.00455, 0.00635 m) They obtained totally 383 data and correlated them based on the criteria for the churn-to-annular flow transition (two test sections of the larger gaps) and the annular-to-annular mist flow transition (the test section with the smallest gap).

Table 1 Previous critical heat flux tests for low-pressure low-flow conditions

References	D_i [m]	D_o [m]	L_h [m]	P [kPa]	G [kg/m^{2}s]	Δh_i [kJ/kg]	q_c [kW/m^2]	Xc [-]
Mishima and Ishii (1982)	0.02045	0.02596	0.5969	101	0~35.8	160~330	44~121	-0.116 ~ 0.859
Rogers et al. (1982)	0.0131	0.0220 0.0250 0.0302	0.480	156	60~1200	180~390	150~2800	-0.13 ~ 0.06
El-Genk et al. (1988)	0.0127	0.0200 0.0218 0.0254	0.5	118	0~260	182~312	155~1418	-0.01 ~ 0.28

An examination of the previous work on the LPLF CHF in annular channels reveals that there still exists a need for further experimental data and reliable prediction models. In this regard, an experimental study on the CHF including two-phase flow visualization has been performed with three vertical annular test sections of different gap sizes under near

atmospheric pressure. Fig. 1 shows the low-pressure CHF test loop of Korea Advanced Institute of Science and Technology (KAIST). Fig. 2 shows the annular test section used in this study with thermocouple locations. It consists of an internally heated stainless-steel tube placed inside the outer transparent unheated Pyrex tube. The heater tube is 0.6 m long, 19 mm O.D. and has a thickness of 1 mm. This tube is screwed and welded into a 19 mm O.D. and 0.12m-long brass rods at both ends, and copper electrodes are attached to the brass rods to provide the electricity from the DC power supply to the heater tube. Each brass rod has a hole of 12 mm diameter along the center line, for an access to the interior of the heater tube for temperature measurement. The wall temperature is measured by 10 Type-K (Chromel-Alumel) thermocouples located on the inner surface of the heater tube. Three different outer tube diameters were used to investigate the effects of the gap size. The test section dimensions are summarized in Table 2.

Table 2 Dimensions of annular test sections used in this study

Test section	D_i (m)	D_o (m)	L_h (m)	D_o/D_i (-)	δ (m)	D_{he} (m)	D_e (m)	L_h/D_{he} (-)	L_h/D_e (-)
TS-1	0.019	0.029	0.6	1.526	0.005	0.02526	0.010	23.753	60
TS-2	0.019	0.035	0.6	1.842	0.008	0.04547	0.016	13.196	37.5
TS-3	0.019	0.051	0.6	2.684	0.016	0.11789	0.032	5.089	18.75

Table 3 summarizes the experimental ranges of parameters for this study. A total of 159 CHF data were obtained for three test sections, including the upward and downward flow conditions. Throughout the experiment, the test section pressure and inlet subcooling were maintained near 110 kPa and 300 kJ/kg, respectively; therefore, the difference in the CHF mainly comes from the differences in the gap width, mass flux, and flow direction. Negative mass fluxes hereinafter indicate the downward flow. The critical quality is the thermodynamic equilibrium quality at the test section outlet, which was calculated by assuming the following steady-state heat balance equation:

$$X_e = \frac{4D_i L_h q_c}{(D_o^2 - D_i^2)Gh_{fg}} - \frac{\Delta h_i}{h_{fg}} \tag{1}$$

It approaches to infinity as inlet mass flux approaches to zero, although the actual quality at the CHF location would not be greater than 1.0 due to the counter-current flow situation.

Table 3 Experimental ranges of parameters

Symbol	D_i (m)	D_o (m)	L_h (m)	P (kPa)	G (kg/m^{2}s)	Δh_i (kJ/kg)	q_c (kW/m^2)	X_e (-)	No. of data
1EU (Up)	0.019	0.029	0.6	110	0 ~ 198.8	295 ~ 337	44.7 ~ 541.7	> -0.029	34
1ED (Down)	0.019	0.029	0.6	110	-120.6 ~ -17.5	302 ~ 324	65.3 ~ 335.1	> -0.119	11
2EU (Up)	0.019	0.035	0.6	110	0 ~ 107.6	292 ~ 325	57.5 ~ 483.7	> -0.030	38
2ED (Down)	0.019	0.035	0.6	110	-91.3 ~ -2.0	302 ~ 334	37.6 ~ 329.5	> -0.063	30
3EU (Up)	0.019	0.051	0.6	110	0 ~ 59.7	292 ~ 317	68.9 ~ 552.9	> -0.053	38
3ED (Down)	0.019	0.051	0.6	110	-46.8 ~ -3.4	302 ~ 333	93.7 ~ 424.4	> -0.055	8

Experimental Results and Discussion

The 97 CHF data (that were selected from 159 data to provide a reasonable parameter distribution) measured in this study are tabulated in Appendix for future use by those who will develop prediction methods. The overall behavior of the CHF and the critical quality is shown in Figs. 3 and 4 as functions of the mass flux.

1 Parametric Trends of Data

(a) Effect of Mass Flux

For given geometry and flow direction, the CHF increases monotonously with the increase of the mass flux (Fig. 3). The rate of the CHF increase seems to be a decreasing function of the mass flux. The critical quality decreases with the increase of the mass flux but the rate of decrease becomes very small near the critical quality of zero (Fig. 4). The CHF at very low flow rate occurs due to the counter-current flow limitation (CCFL) or flooding. However, the zero flow CHFs are not properly represented by the following Wallis' flooding correlation (Block and Wallis, 1978):

C was found to be 0.57, 0.43, and 0.25 for TS-1, TS-2 and TS-3, respectively, while it was reported as 0.8 for the narrower test section of Mishima and Ishii (1982). The decrease of C with the increase of δ would be due to the increased imbalance of liquid distribution and enthalpy between the inner and outer wall sides.

$$q_{c,G=0} = \frac{A_f}{A_h} \frac{C^2 h_{fg} \sqrt{\rho_g g \Delta\rho D_e}}{[1+(\rho_g/\rho_f)^{1/4}]^2} \tag{2}$$

The overall effect of the mass flux is very similar to the findings by previous investigators (Rogers et al. 1982; El-Genk et al., 1988) and also generally similar to that for round tubes (Chang et al., 1991).

(b) Effect of Flow Direction

Although the flow was maintained stable for both upward and downward flow conditions, somewhat lower CHF values were observed for the downward flow with the difference up to 30%. This comes from the effect of gravity that hinders the escape of vapor bubbles from the test section for downward flow condition and becomes large at low flow and low pressure conditions. The effect of the flow direction on the LPLF CHF in annuli has not been reported before but the present work shows that it is considerably larger than that observed for round tubes (Mishima et al., 1985; Chang et al., 1991). This would be related to the difference in flow regimes between the round tube and the annulus with an unheated outer wall.

(c) Effect of Gap Width

For the same inlet mass flux and subcooling, the CHF increases with the increase of the gap width (Fig. 3). This is related to the fact that the enthalpy increase becomes smaller for the larger gap width at a given heat flux condition. The critical quality decreases with the gap width though the difference is not so great as that in the CHF itself (Fig. 4). This may be due to that the liquid fraction on the unheated outer wall increases with the increase of the gap.

2 Comparison with Previous Work

Fig. 5 compares the CHF data for upward flow with the data of Mishima and Ishii (1982), Rogers et al. (1982), and El-Genk et al. (1988). Though a direct quantitative comparison is not easy due to the differences in test section dimensions and inlet flow conditions, the overall trend of the CHF with the mass flux is similar for all the data sets. In particular, the conditions of Mishima and Ishii (1982) are very similar to the present study except for the gap size. The smaller CHF values of Mishima and Ishii (1982) are consistent with the parametric effects found in this study.

When compared with the LPLF CHF data for round tubes (Mishima et al., 1985; Chang et al., 1991), the parametric effects of mass flux, hydraulic diameter ($D_e = 2\delta$) and flow direction on the CHF and critical quality are similar to those for round tubes from the viewpoint of fixed inlet conditions, though the flow direction effect is much larger for annuli, as discussed in the previous section. The most overriding difference in the CHF behavior between annuli and round tubes would be the much lower critical quality measured in annuli. As the liquid flowing along the unheated outer wall is not very effective in cooling the heated surface, the CHF could occur at the lower value of the channel-average enthalpy. This is conceptually illustrated in Fig. 6 which compares the critical quality data between annuli and round tubes for the same hydraulic equivalent diameter of 10 mm.

The location of CHF occurrence agrees with previous understanding. In upward flow tests, the CHF occurred at downstream end (i.e., at the top), except for very low flow conditions of G < 20kg/m^{2}s where flooding was the CHF mechanism. In downward flow tests, the CHF always occurred at downstream end, i.e., at the bottom.

3 Visual Observations

Visual observations, supported by high-speed camera and video system, consistently reveal the presence of either a churn- or an annular flow near the CHF location.

At very low upward flow, a stable annular flow was established with continuous liquid films on both inner an outer walls. The outer liquid film was generally thicker than the inner film. At flow rates near zero, the liquid film flows in downward direction and the CHF occurred due to flooding. At a little higher upward flow rates, the liquid film flows upward and the CHF occurred when the inner liquid film on the heated wall was fully evaporated at the top.

At higher upward flow, the flow pattern just before the CHF occurrence was either slug or churn flow. When the heat flux was further increased at this situation, the annular-like flow regime was developed and progressed from the top to the bottom of the test section within a few seconds, and the dryout of the liquid film occurred near the top of the heater tube. The direction of liquid film flow during this transition was observed to be downward. This CHF mechanism can be ascribed to the churn-to-annular flow transition as reported by previous workers (Mishima and Ishii, 1982; El-Genk et al., 1988).

When the flow rate was increased further, the CHF occurred near the top of the test section as a result of local dryout of liquid film from the churn or slug flow regime, accompanying a large fluctuation of heater surface temperatures. This is a

kind of departure from nucleate boiling (DNB) rather than annular film dryout (AFD) observed for other cases. The minimum mass flux for this DNB-type CHF decreased with the increase of the annular gap width.

The flow characteristics were different for downward flow condition due to the effect of gravity. The liquid flow was always in downward direction regardless of the flow rate and flow regime, resulting in the first occurrence of the CHF near the bottom of the test section. The direction of vapor flow depended on the mass flux: upward for low $|G|$ and downward for higher $|G|$.

Due to the interference by the outer Pyrex tube, the quality of pictures taken by the high speed camera system is not so good to reproduce here, though the flow regime is clearly shown by the use of a VCR (Fig. 7).

Conclusions

This paper has presented the results of CHF tests for water flow in vertical, internally heated, concentric annuli at LPLF conditions, which expands the existing data base especially for large gap sizes and downward flow that are not properly covered by existing data bases. Following conclusions can be drawn from this study:

(a) The observed parametric trends based on fixed inlet conditions are generally consistent with previous understanding: the increase of the CHF and the decrease of the critical quality with the increase of mass flux, the higher CHF and the lower critical quality for the larger gap width, decreasing trends of mass flux effects on the CHF and critical quality with the increase of mass flux, etc.

(b) The CHF for downward flow is significantly lower (up to 40%) than that for upward flow at the same inlet conditions, unlike the behavior in round tubes which shows little difference.

(c) The critical quality is much lower than that for round tubes at the same inlet conditions (i.e., D_e or D_{he}, L_h, G, Δh_i) due to the effect of the unheated outer wall. When the data at zero flow conditions are fit with the Wallis flooding correlation, the constant C is a decreasing function of the gap width.

(d) The CHF mechanism changes in the order of flooding, churn-to-annular flow transition, and local large bubble formation in churn flow as the flow rate was increased from zero to higher values.

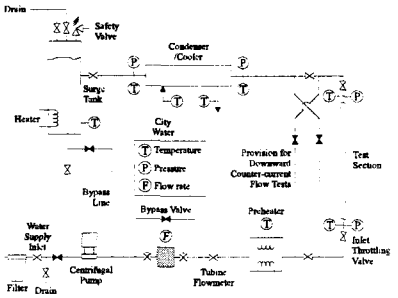

Fig. 1. Schematic diagram of experimental loop

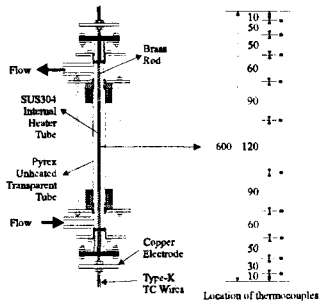

Fig. 2. KAIST annuli test section

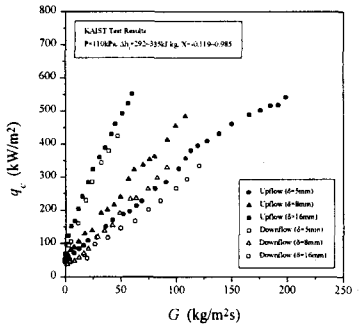

Fig. 3. Parametric trend of CHF vs. mass flux

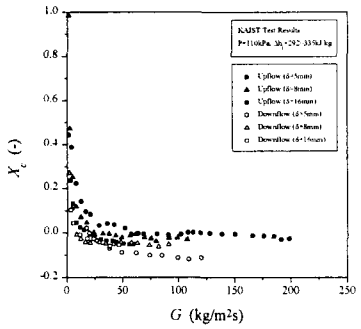

Fig. 4. Parametric trend of X_c vs. mass flux

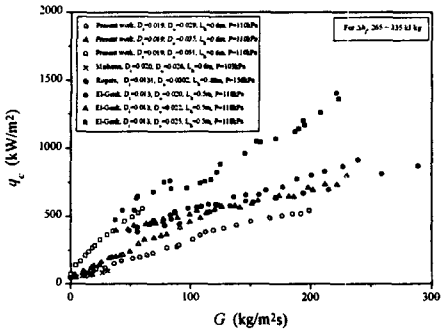

Fig. 5. Comparison with existing LPLF CHF data

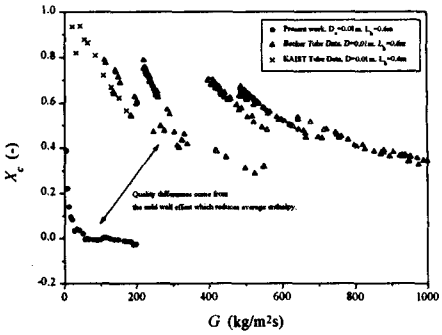

Fig. 6. Comparison of the critical quality between annuli and round tubes for the same hydraulic equivalent diameter of 10 mm

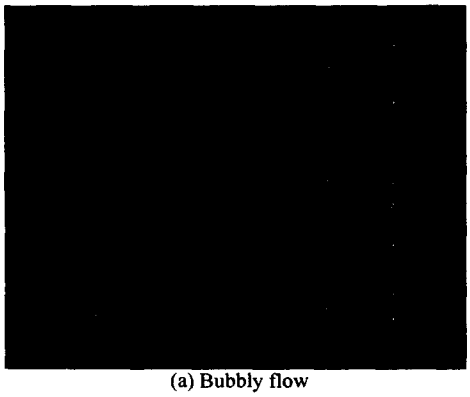

(a) Bubbly flow

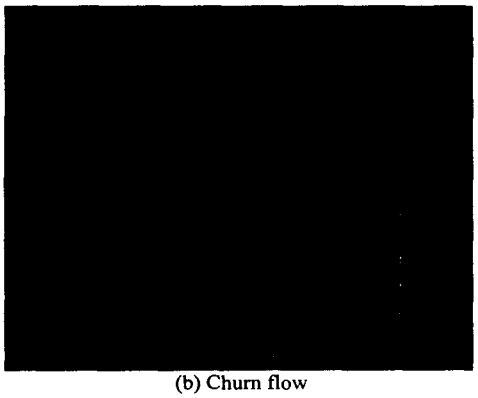

(b) Churn flow

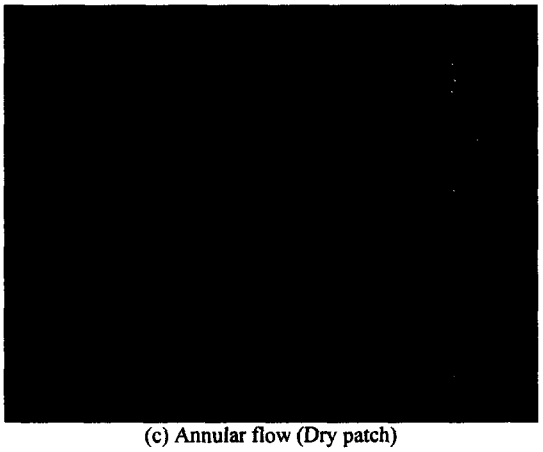

(c) Annular flow (Dry patch)

Fig. 7. Photographs of flow patterns during CHF experiments

Appendix. Table of Measured CHF Data

D_i	D_o	L_h	P	G	Δh_i	q_c	X_c
0.019	0.029	0.6	110	0	336.5	44.7	--
0.019	0.029	0.6	110	4.2	307.3	52.2	0.388
0.019	0.029	0.6	110	8.4	309.8	71.5	0.222
0.019	0.029	0.6	110	12.6	318.1	84.3	0.141
0.019	0.029	0.6	110	16.8	316.5	93.8	0.095
0.019	0.029	0.6	110	21.0	308.1	109.2	0.083
0.019	0.029	0.6	110	28.6	317.7	118.1	0.033
0.019	0.029	0.6	110	36.0	305.2	150.8	0.041
0.019	0.029	0.6	110	42.3	302.3	170.3	0.036
0.019	0.029	0.6	110	51.8	298.1	187.1	0.020
0.019	0.029	0.6	110	57.6	334.4	195.5	-0.005
0.019	0.029	0.6	110	63.7	326.1	213.6	-0.003
0.019	0.029	0.6	110	68.6	325.6	227.6	-0.005
0.019	0.029	0.6	110	80.4	326.9	265.3	-0.006
0.019	0.029	0.6	110	90.5	322.7	285.1	-0.010
0.019	0.029	0.6	110	102.0	316.9	326.7	-0.006
0.019	0.029	0.6	110	108.2	309.8	357.4	0.002
0.019	0.029	0.6	110	112.8	316.5	381.1	0.002
0.019	0.029	0.6	110	119.2	312.3	395.4	1E-3
0.019	0.029	0.6	110	127.8	308.1	410.5	-1E-3
0.019	0.029	0.6	110	138.6	308.5	432.8	-0.005
0.019	0.029	0.6	110	150.0	305.2	461.8	-0.006
0.019	0.029	0.6	110	166.0	305.6	488.6	-0.012
0.019	0.029	0.6	110	176.0	302.3	502.6	-0.014
0.019	0.029	0.6	110	185.0	302.3	516.6	-0.016
0.019	0.029	0.6	110	191.9	321.5	517.7	-0.029
0.019	0.029	0.6	110	198.8	316.9	541.7	-0.026
0.019	0.029	0.6	110	-17.5	309.4	65.3	0.02
0.019	0.029	0.6	110	-20.0	314.4	55.8	-0.002
0.019	0.029	0.6	110	-27.1	308.5	97.8	-0.035
0.019	0.029	0.6	110	-38.5	316	117.3	-0.069
0.019	0.029	0.6	110	-49.5	324	145.2	-0.088
0.019	0.029	0.6	110	-62.5	301.8	167.5	-0.09
0.019	0.029	0.6	110	-74.5	312.7	201.0	-0.102
0.019	0.029	0.6	110	-85.5	303.1	228.9	-0.102
0.019	0.029	0.6	110	-99.5	316	265.3	-0.113
0.019	0.029	0.6	110	-109.5	324	293.2	-0.119
0.019	0.029	0.6	110	-120.5	301.8	335.1	-0.111
0.019	0.035	0.6	110	0.0	312.3	57.5	--
0.019	0.035	0.6	110	1.3	311.9	62.3	0.985
0.019	0.035	0.6	110	2.5	324.8	65.7	0.472
0.019	0.035	0.6	110	4.9	296.8	79.8	0.250
0.019	0.035	0.6	110	8.2	303.5	88.3	0.118
0.019	0.035	0.6	110	12.3	294.7	105.5	0.070
0.019	0.035	0.6	110	17.2	296.8	123.1	0.036
0.019	0.035	0.6	110	23.8	303.5	137.9	0.001
0.019	0.035	0.6	110	31.9	324.8	190.8	-0.004
0.019	0.035	0.6	110	37.5	294.7	201.2	-0.005
0.019	0.035	0.6	110	43.4	291.8	215.9	-0.013
0.019	0.035	0.6	110	49.2	303.5	238.3	-0.021
0.019	0.035	0.6	110	56.5	305.2	292.8	-0.014
0.019	0.035	0.6	110	61.5	291.8	322.8	-0.007
0.019	0.035	0.6	110	69.6	303.5	336.6	-0.021
0.019	0.035	0.6	110	75.5	305.2	353.2	-0.026
0.019	0.035	0.6	110	80.2	324.8	362.6	-0.038
0.019	0.035	0.6	110	91.5	292.6	413.6	-0.024
0.019	0.035	0.6	110	99.0	291.8	455.2	-0.022
0.019	0.035	0.6	110	107.8	303.5	483.7	-0.03
0.019	0.035	0.6	110	-2.1	334.4	37.6	0.271
0.019	0.035	0.6	110	-4.2	309.4	44.2	0.109
0.019	0.035	0.6	110	-8.4	316.0	46.9	-0.009
0.019	0.035	0.6	110	-12.6	301.8	57	-0.028
0.019	0.035	0.6	110	-16.8	316.0	69.8	-0.043
0.019	0.035	0.6	110	-21.0	314.4	83.8	-0.046
0.019	0.035	0.6	110	-29.4	312.7	119.5	-0.044
0.019	0.035	0.6	110	-34.8	316	136.2	-0.049
0.019	0.035	0.6	110	-42.0	309.4	153.4	-0.052
0.019	0.035	0.6	110	-48.6	301.8	190.5	-0.042
0.019	0.035	0.6	110	-58.1	312.7	232.7	-0.045
0.019	0.035	0.6	110	-63.4	303.1	234.8	-0.048
0.019	0.035	0.6	110	-74.0	316	262.7	-0.057
0.019	0.035	0.6	110	-82.4	333.2	297.3	-0.063
0.019	0.035	0.6	110	-91.3	309.4	329.5	-0.053
0.019	0.051	0.6	110	0.0	297.7	68.9	--
0.019	0.051	0.6	110	1.5	307.7	96.3	0.444
0.019	0.051	0.6	110	3.0	304.3	122.3	0.234
0.019	0.051	0.6	110	5.2	296.8	151.1	0.131
0.019	0.051	0.6	110	8.4	304.3	167.3	0.045
0.019	0.051	0.6	110	11.5	309.4	203.8	0.023
0.019	0.051	0.6	110	15.1	296.8	240.1	0.012
0.019	0.051	0.6	110	20.3	301.8	282.8	-0.008
0.019	0.051	0.6	110	24.6	304.3	323.9	-0.016
0.019	0.051	0.6	110	30.6	309.3	360.2	-0.031
0.019	0.051	0.6	110	35.5	304.3	388.1	-0.036
0.019	0.051	0.6	110	41.2	294.7	429.9	-0.037
0.019	0.051	0.6	110	44.7	301.8	460.7	-0.041
0.019	0.051	0.6	110	51.1	307.7	491.4	-0.05
0.019	0.051	0.6	110	56.2	309.4	522.1	-0.053
0.019	0.051	0.6	110	59.7	304.3	552.9	-0.051
0.019	0.051	0.6	110	-3.4	333.2	93.7	0.101
0.019	0.051	0.6	110	-5.3	309.4	105.3	0.042
0.019	0.051	0.6	110	-11.5	301.8	159.5	-0.009
0.019	0.051	0.6	110	-18.5	312.7	228.9	-0.027
0.019	0.051	0.6	110	-24.2	303.1	284.8	-0.028
0.019	0.051	0.6	110	-32.5	316.0	343.4	-0.045
0.019	0.051	0.6	110	-38.9	333.2	379.7	-0.06
0.019	0.051	0.6	110	-46.8	309.4	424.4	-0.055